Ref. Ares(2019)1461213 - 04/03/2019

HORIZON 2020

IMMERSE

(Grant Agreement 821926)

Improving Models for Marine EnviRonment SErvices

Deliverable D6.1 Public type

2

I. Introduction

The IMMERSE program is a research project which aims to prepare numerical ocean models for the next generation of Copernicus Marine Environment Monitoring Service (CMEMS). The IMMERSE program integrates several activities ranging from NEMO ocean model core development to demonstration for CMEMS users. The present work is part of the work package 6 (WP6) of the program called "Demonstrating impact of NEMO developments on CMEMS model-based systems". The general aim of WP6 is to demonstrate the impact of NEMO code developments undertaken in IMMERSE on prototype NEMO configurations, which could prefigure the future CMEMS systems. In particular, this work focuses on the impact of increasing the resolution in CMEMS regional Monitoring Forecasting Centre (MFC).

The regional MFC component selected for WP6 is the Iberian – Biscay – Irish (IBI) MFC (Maraldi et al, 2013). It provides daily ocean model estimates and forecasts of diverse physical parameters at a 1/36° resolution for the IBI regional seas since 2011. Until 2024, the IBI-MFC system will be facing some major upgrade such as an improvement of the assimilation method, upgrade of the NEMO version, extension of the horizontal grid. The present work aims at prefiguring the N+2 (i.e: after 2024) version of the IBI forecasting system.

In this framework, IBI-MFC configurations will benefit from an increase of the horizontal resolution towards a kilometric resolution scale. Indeed, such a resolution allows a better representation of the mesoscale structures in the IBI area, which has a complex topography leading to a large variety of scales for the mesoscale structures. For example, the first baroclinic Rossby radius of deformation (which defines the scale of the mesoscale eddies in the ocean) is over 20km in the southwestern part of the IBI area, less than 10km in the Mediterranean Sea and less than 2km over the continental shelf (see 1 in sec II.A). At a resolution of 2-3km (1/36°), the mesoscales structures are typically poorly resolved (2 to 3 points) in the Mediterranean Sea and not resolved at all over the continental shelf.

In this context, this IMMERSE deliverable (6.1) presents the implementation of a high (kilometric) resolution nest over the IBI configuration based on last version of NEMO, which incorporates improved physics and HPC developed in IMMERSE. This deliverable has two objectives: the first is to describe the configuration, its setup and pre-processing tools are described, then second is to present a macroscopic validation of the new NEMO code and of the high-resolution nested configuration.

II. Configurations

A. eNEATL36

The configuration used as parent for the high-resolution nest is called eNEATL36 (extended North-East ATLantic). It is an extended version of the IBI (Iberian, Biscay, Ireland) configuration (Maraldi et al., 2013) over the western Mediterranean Sea to the strait of Sicily (1). It has a 1/36° resolution, 50 (geopotential) vertical levels and a baroclinic time step of 150s. The vertical z* coordinate used here (Adcroft and Campin, 2004) evolves according to the free-surface as usual, but benefits from a new and more efficient implementation developed in the frame of the project (it stands as the Quasi-Eulerian vertical Coordinate (QCO option in NEMO). The temporal and spatial parameters of the eNEATL36 configuration are sumarized in Table 1.

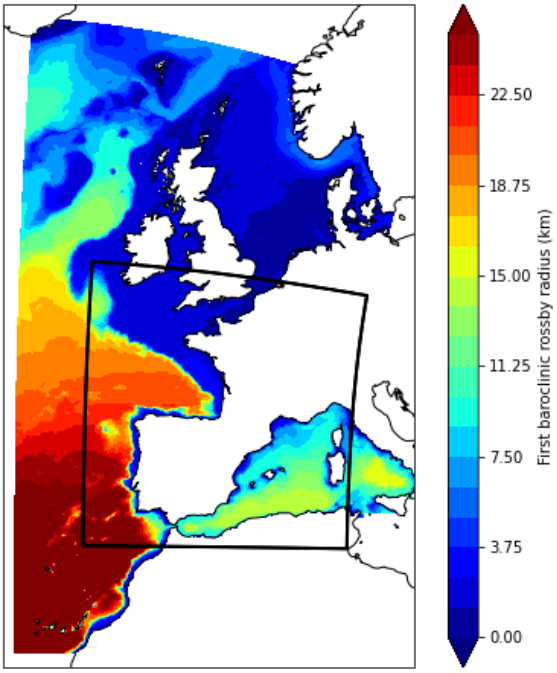

Figure 1: First baroclinic Rossby radius over the eNEATL36 area. The black frame displays the area covered by the high resolution AGRIF nest.

Atmospheric forcing are provided by the ECMWF's Integrated Forecasting System (IFS) model at hourly frequency and at a resolution of ~8km. The surface turbulent fluxes are computed from 10m winds and 2m air temperature and humidity using the ECMWF bulk algorithm included in NEMO (Brodeau et al., 2017) and the radiative fluxes are prescribed from IFS. The penetrative radiative forcing is parameterized with a red-green-blue penetrative scheme with a constant chlorophyl value. The initial state and the lateral boundary conditions are given by the 1/12° global analysis PSY4V3R1 (Lellouche et al., 2018). At the parent domain boundaries, explicit tidal forcing is also provided for 11 harmonics (M2, S2, N2, K1, O1, Q1, M4, K2, P1, Mf, Mm) by the FES2014 global ocean tide atlas (Lyard et al., 2021).

The runoffs used for the eNEATL36 configuration are derived from the runoff data used in previous IBI configurations (Maraldi et al., 2013). Freshwater inputs derived from a blended product of observations (PREVIMER) and simulated data (SMHI E-HYPE) are prescribed for 33 rivers over the eNEATL36 area. In addition, a climatology of monthly freshwater discharge from watersheds is also prescribed to the model (see also sec. II.B.3). Note that the river runoff inputs are prescribed as precipitation into the model, which is different than in Maraldi et al., (2013) where they are prescribed as boundary conditions (see sec. II.C.3).

The simulation also includes new schemes and parameterisations developed in the frame of the IMMERSE program, such as the new current feedback parameterisation scheme (Renault et al., 2017), the new skin Sea Surface Temperature (SST) parameterisation and the new fourth order advection scheme (see Madec et al., 2022).

The increase of horizontal resolution via the nested configuration was also the opportunity to upgrade the eNEATL36 bathymetry towards a higher resolution (and more recent) CMEMS product. Thus, the NEMO bathymetry files for the configuration are constructed from the recent high-resolution bathymetry dataset EMODnet 2018 (EMODnet Digital Bathymetry (DTM 2018), 2022) which has an hectometric resolution. The construction and pre-processing of the bathymetry file are described in sec II.C.1.

	eNEATL36	BIzoo
Horizontal resolution (°)	*1/36*	*1/108*
Horizontal resolution (km)	*~3*	*~1*
Temporal resolution (s)	*150*	*50*
N° of points	*2 450 836*	*6 870 915*
Area covered (km²)	*11 720 351*	*3 830 553*
N° of vertical levels	*50*	*50*
Longitude (min)	*-19.91*	*-11.86*
Longitude (max)	*22.67*	*11.29*
Latitude (min)	*26.10*	*33.67*
Latitude (max)	*64.15*	*56.70*

Table 1 : Main characteristics of the parent (eNEATL36) and child (Bizoo) domains.

B. Nested configuration (eNEATL36 + Bizoo)

The configuration eNEATL36 + Bizoo (Biscay ZOOm) is based on the post-IMMERSE version (branch 4.2.0 of the NEMO git : https://forge.nemo-ocean.eu/nemo/nemo.git%20nemo_4.2.0) of the NEMO model (NEMO 4.2, Madec et al., 2022). It uses eNEATL36 as parent configuration and includes a 1/108° (kilometric resolution) nest that covers the Atlantic and Mediterranean French and Iberian coasts and includes the Gibraltar Strait, Corsica, and Sardinia (1). The nesting is done thanks to the AGRIF (Adaptive Grid Refinement In Fortran) library (https://sites.nemo-ocean.io/user-guide/zooms.html; Debreu and Blayo, 2008) which allow space and time refinement of rectangular regions in NEMO. A major particularity of this configuration is that the interactions between the parent and the child grids are two-way: the parent grid feeds the child grid open boundaries, and the child provides volume/area weighted averages of prognostic variables once a given number of time steps are completed. At the beginning of a baroclinic parent time-step, the barotropic mode is computed over the parent domain to set up the barotropic forcing on the overlapping zone. Then, the model iterates over the nest barotropic and baroclinic time steps and AGRIF finally updates the parent solution of the nest area with the weighted average of the child solution. Consequently, both the child and the parent model solution are consistent over the overlapping zone.

The nest baroclinic time step is 50s and it has the same number of vertical levels as in the parent configuration (eNEATL36). It also uses the same parameterisations and type of vertical coordinate (QCO) as eNEATL36, and the nest is initialized by the same initial state as for the parent domain. The temporal and spatial parameters of the nested configuration are presented in Table 1.

For stability issues (e.g. CFL violations at a few coastal points), a regional boost is used on the bottom drag coefficient over the bay of Mont St Michel and the bay of Bristol (**Erreur ! Source du renvoi introuvable.**). Over those areas, the bottom drag coefficient is multiplied by 2 (it remains unchanged elsewhere).

The configuration description are available on the IMMERSE GitHub: https://github.com/immerse-project/eNEATL36-BIzoo_Demonstator and was delivered through the milestone M30.

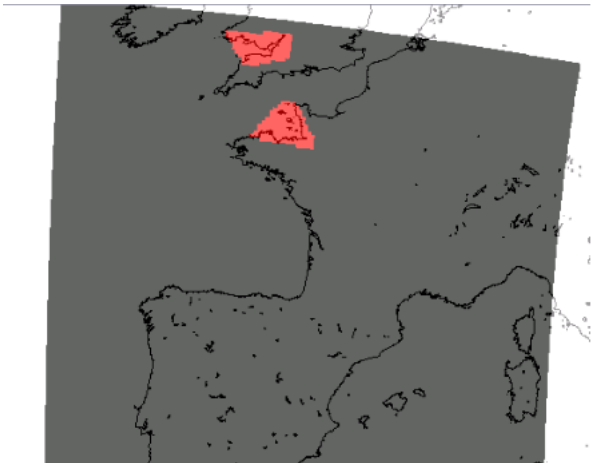

Figure 2: Maps of the regions where a regional ×2 boost is used on the bottom drag coefficient (in red)

C. Setup of the nested configuration

1. Bathymetry

The current bathymetry used for standard IBI configurations is derived from the 30 arc-second resolution GEBCO 08 dataset. However, the development of the high resolution eNEATL36 + Bizoo configuration in the context of IMMERSE is the opportunity to upgrade the bathymetry towards a higher resolution CMEMS product.

The dataset chosen to construct the eNEATL36 + Bizoo configurations is derived from the 1/16 arc-minute (~115m) resolution EMODnet 2018 dataset (DOI:10.12770/18ff0d48-b203-4a65-94a9-5fd8b0ec35f6). EMODnet 2018 digital bathymetry (DTM) covers the whole eNEATL36 area and is constructed from 9400 bathymetric survey datasets and composite DTMs, gathered from 24 countries, and from satellite-derived bathymetry products. The water depth in EMODnet is referring to the Lowest Astronomical Tide (L.A.T) and is gridded on a DTM grid.

In NEMO, bathymetry should be referenced to the mean sea level (see Figure 3). Since the EMODnet 2018 bathymetry is referenced to the L.A.T, some treatments are necessary to the bathymetry file. First, the bathymetry over the child domain is obtained by interpolating EMODnet 2018 tiles data (which can be downloaded at this link: https://portal.emodnet-bathymetry.eu/?menu=19) on the 1/108° AGRIF grid using the new NEMO 4.2 DOMAINcfg tool.

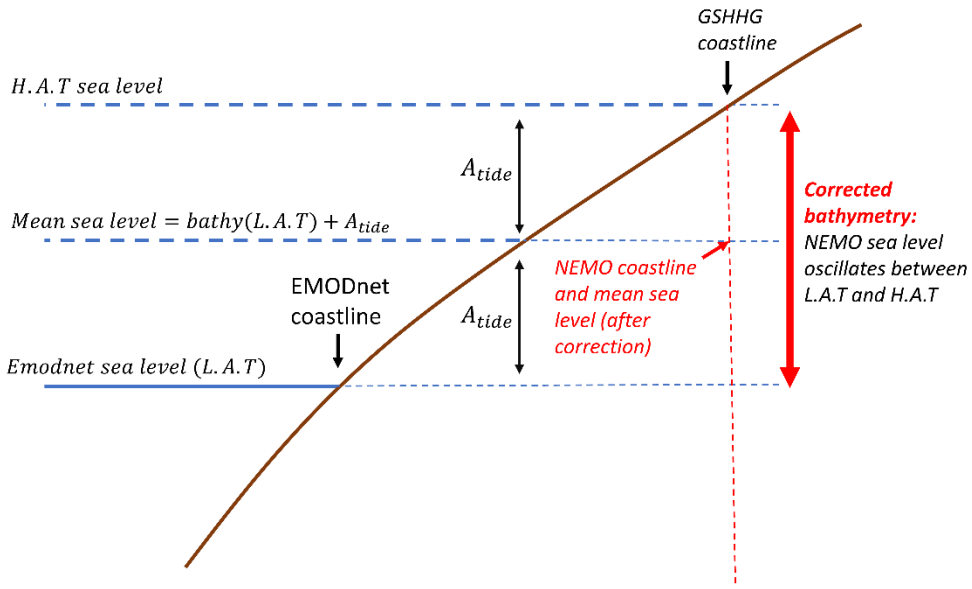

Figure 3 : schematic representation of a 2d x-z ocean slice near the coastline (brown line), with different sea level references (blue lines): H.A.T (Highest Astronomical Tide), L.A.T (Lowest Astronomical Tide) and mean sea level. A_{tide} is the tide amplitude.

The coastline is then corrected using the BathyMeshGrid (BMG) tool developed at IFREMER (Theeten et al., 2014). For this, we use the GSHHG (Wessel et al. 1996) coastline dataset which corresponds to the H.A.T (Figure 4). Finally, as a proxy of the tidal amplitude, we used the sum of S2 and M2 tidal harmonics computed from the FES2014 (Lyard et al. 2021) dataset, which is simply added to the bathymetry.

This treatment was done only on the nest (Bizoo) bathymetry for practical reasons: for the eNEATL36 grid, the NEMO input bathymetry file based on EMODnet 2018 and the corresponding tidal forcing files were already available and validated (see the K. Guillou technical report on the new EMODnet2018 – based bathymetry for eNEATL36 on the IMMERSE GitHub : https://github.com/immerse-project/eNEATL36-BIzoo_Demonstator/blob/main/DOC/bathy_K_guillou_technical_report_2021.pdf). As updating a bathymetry of a regional configuration require a recalculation of the tidal forcing, we choose not to update the bathymetry over the parent domain and to directly use the EMODnet2018-based eNEATL36 bathymetry file. However, it is important to note that the treatment made on this eNEATL36 bathymetry file is different than our treatment: the bathymetry is also corrected with a coastline referenced to H.A.T, but the tidal amplitude is not added to the data. A threshold is however applied to the bathymetry so that the minimum water height is higher than the tidal amplitude. This imply that the bathymetry is slightly deeper over regions of strong tides in the eNEATL36 + Bizoo configuration than in eNEATL36-only configurations.

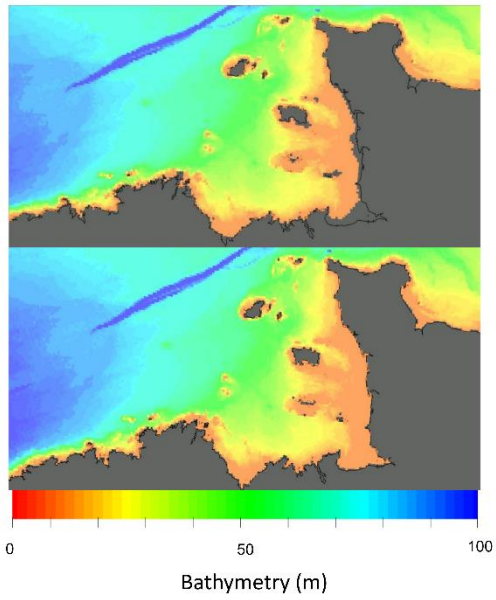

Figure 4 : EMODNET2018 bathymetry uncorrected (top) and corrected with the BMG tool. The GSHHG coastline trait is represented in dark.

2. *NEMO coordinate files*

Since the version 4.0 of NEMO, the model requires input coordinate files (domain_cfg.nc files) that must be created beforehand with the new DOMAINcfg tool. For NEMO + agrif simulations, the tool must be compiled with the cpp key “key_agrif”.

The creation of the coordinate files for the eNEATL36 + Bizoo configuration requires several steps. The first step is to create a domain_cfg_init.nc file for the eNEATL36-only configuration. For this, we compile the DOMAINcfg tool without “key_agrif”. At this step, the tool only requires a bathymetry and a coordinate file that contains the latitude and the longitude of the grid points. In our case, we use the NEMO bathymetry file based on the EMODnet 2018 dataset created by Guillou (2017) (see sec II.B.1).

The DOMAINcfg tool is then compiled with “key_agrif” to create a first set of coordinate files for the eNEATL36 + Bizoo configuration. Several input files are required at this step:

- The domain_cfg_init.nc file (created from the previous step) which is read by the tool to set up the vertical coordinates and the land-sea mask of the parent configuration outside the nest area and over the first 4 overlapping points.
- An external bathymetry dataset (on a regular grid) from EMODnet 2018.
- The AGRIF_FixedGrids.in file, that contains the coordinates of the first and last points on the parent grid and the refinement factors.

First, the tool reads and interpolates the external bathymetry dataset on the child grid. The child bathymetry is then extrapolated on the parent grid using a median average. The tool ensures the volume consistency between the child and the parent grid over the nest area. Near coasts, the parent grid points are masked when they cover at least one land point of the child grid. Outside the nest area, the 3D coordinates are simply read in the domain_cfg_init.nc file.

In the last step, the bathymetry of the child domain is updated as described in II.C.1 directly in the NEMO coordinate file. The DOMAINcfg is then used one last time to recompute the parent and child model coordinate files from the updated bathymetry on the child grid.

3. *Runoffs*

- *River inputs*

In NEMO, runoffs can be prescribed to the ocean in two different ways. The first method is to prescribe runoffs as precipitation (in kg/m²/s) and was used in previous IBI configurations to prescribe the watersheds discharge to the ocean. In the second method, the river discharge is prescribed configuration as a flux (boundary conditions in m^3/s).

The current version of the AGRIF code is not compatible with boundaries within the child domain. To overcome this limitation, river freshwater inputs (in m^3/s) prescribed as BDY (RNF_{bdy}) are converted into 2-dimensional runoff data (RNF_{rain}, in kg/m²/s) and prescribed as rain following:

$$RNF_{rain} = \frac{RNF_{bdy} * \rho_{freshwater}}{e1t * e2t}$$

Where $\rho_{freshwater} = 1000\ kg/m^3$ and $e1t$, $e2t$ are the mesh size along x and y direction.

The volume of water brought into the ocean by the runoffs is slightly different between the two methods (i.e : prescribing RNF_{rain} or RNF_{bdy}). Indeed, rivers applied are applied as BDY by specifying a Neumann condition for the temperature and a constant salinity of 0.1 psu, resulting in a salinity and heat input different than when the freshwater input is prescribed as a surface flux. However, prescribing RNF_{rain} instead of RNF_{bdy} only has a slight and localised impact on the SST and SSS at small scales (see Figure 5) and does not affect the mean state of these variables. Thus, changing the way we prescribe runoffs into the model does not have a significant impact on the water volume.

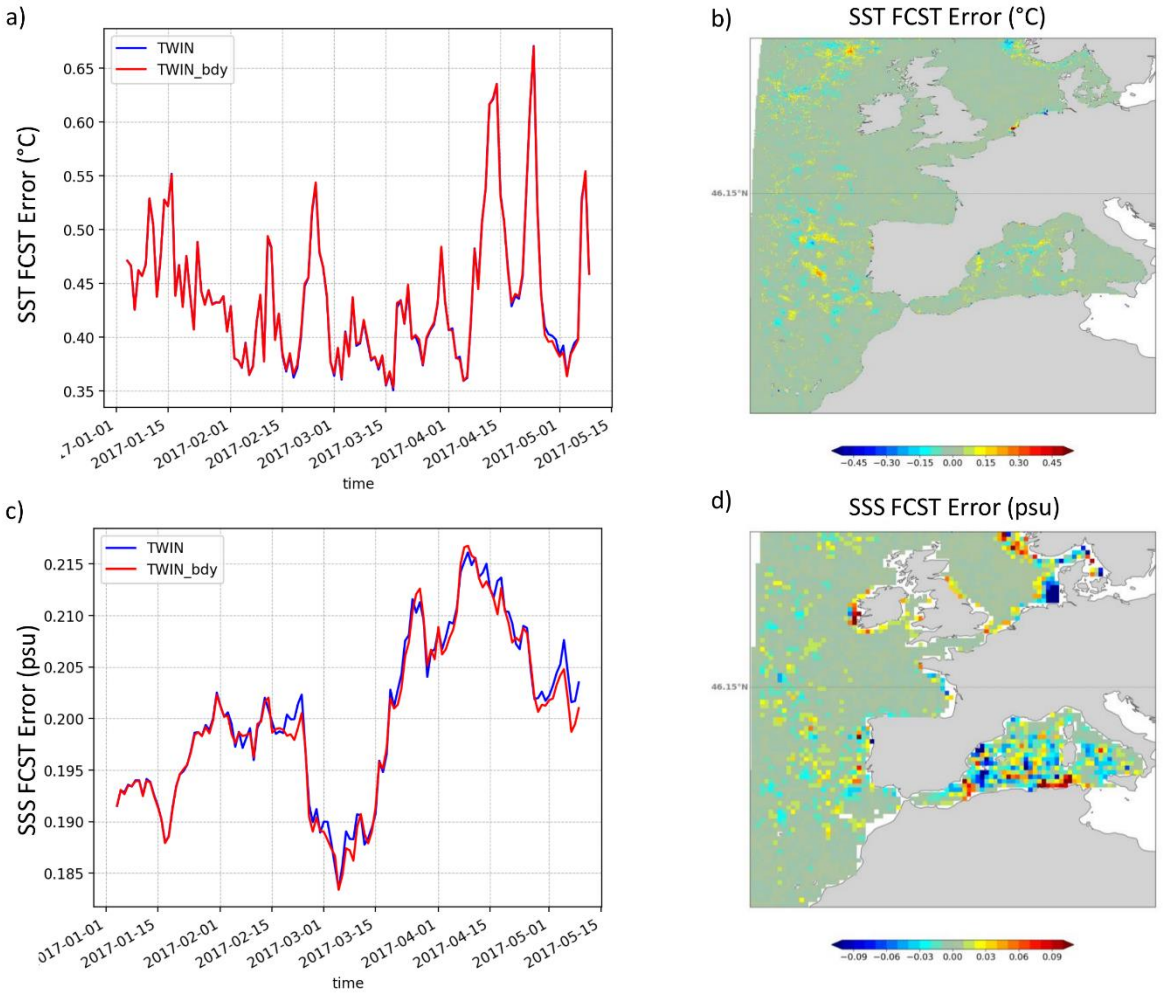

Figure 5 : a), c): Time series of the mean Forecast error (=abs(obs – model)) on SST (°C) and SSS (psu), averaged over the eNEATL36 area for a simulation (TWIN) on the eNEATL36 configuration (blue) in which the rivers are prescribed to the ocean as rain and for a simulation (TWIN_bdy) in which the rivers are prescribed as boundary condition (red). B), d): 2D Maps of the mean forecast error on SST (b) and SSS (d) difference between TWIN and TWIN_bdy over the 2017-01-04 – 2017-05-15 period.

- *Replacing the runoffs on the updated eNEATL36 coastline*

Over the parent domain, the eNEATL36 + Bizoo coastline has changed from previous eNEATL36 configurations because of the use of a new bathymetry and the update of the parent domain in AGRIF. Therefore, we use a python program to automatically replace 2D runoffs (i.e: the watershed runoffs) alongside the coast. The program consists in an algorithm that select all runoffs points surrounded by land or by sea, finds the nearest coast point and append the weighted runoff value to this point (the runoff value of the point at the previous position is set to 0). The nearest coast point is selected preferentially along x and y direction, and then diagonally if no point is found. When more than one coast point nearby is found, the program dispatches the runoff value between all these points. The 33 rivers (converted into 2D values) are appended manually afterwards to the 2D runoff data

- *Extrapolation on the child grid*

The runoffs are then interpolated over the child grid with a python program. The program first extrapolates weighted parent runoffs values over the child grid (see step 1 in Figure 6). Then, the runoffs are replaced near the coast (step 2 in Figure 6). The program ensures the total freshwater flux is conserved, so that (over the nest area):

$$\sum(RNF_{child} * e1t_{child} * e2t_{child}) = \sum(RNF_{parent} * e1t_{parent} * e2t_{parent})$$

Where, for both grids ("parent" and "child"), $RNF_{grid\ name}$ is the runoff value and e1t, e2t are the mesh size along x and y direction.

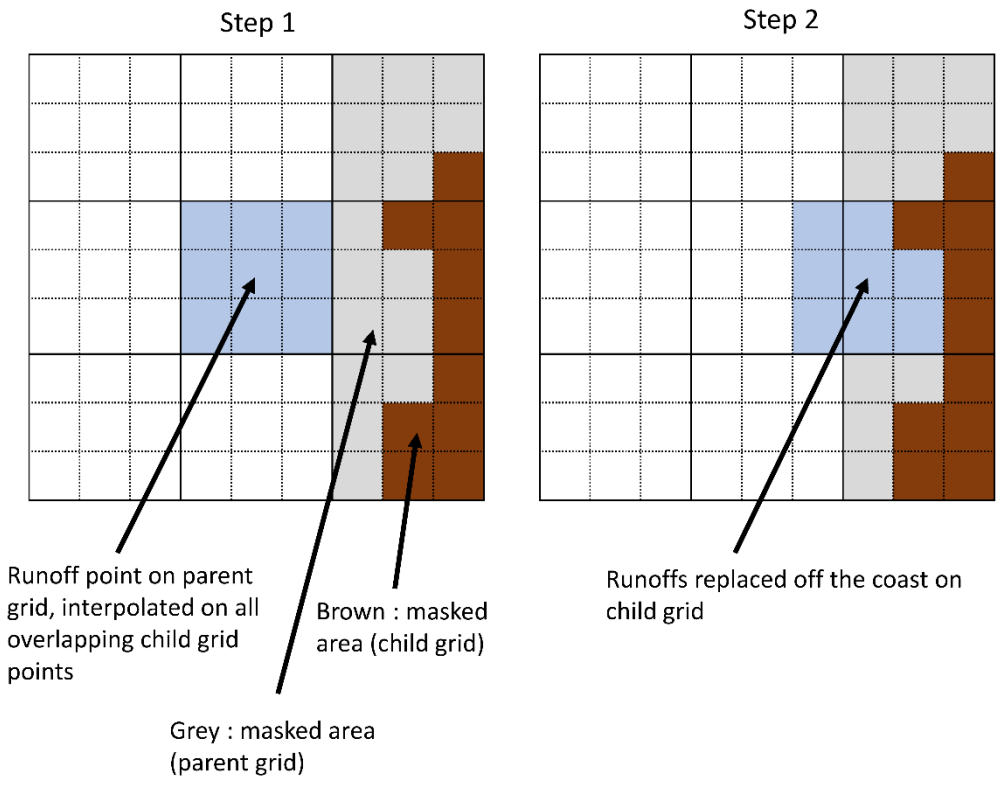

Figure 6 : Schematic representation of the extrapolation of a runoff point from the parent grid to the child grid. Solid lines and dotted lines represent the parent and the child grids respectively.

D. Simulations and observations

- *Demonstrator simulation*

A 1.5-year demonstrator simulation is performed on the eNEATL36 + BIzoo configuration. The simulation covers the period from January 4th, 2017 to June 30th, 2018. This period has been selected to match two in-situ campaigns lead by IMMEDEA (Spain) in July 2017 and in May – June 2018 over the Alboran sea and in the Balearic Sea. 3D outputs of Temperature, salinity, 3D currents and Sea Surface Height (SSH) were saved at a daily frequency. In addition, 2D hourly outputs of SST, SSS (Sea Surface Salinity), surface currents and SSH were saved at hourly frequency.

- *Twin simulation*

A "twin" simulation, called TWIN, is used to validate the demonstrator simulation. It covers the same period, uses the same initial conditions, lateral and atmospheric forcing, parameterizations, and physical schemes as for the eNEATL36 + Bizoo demonstrator. The major difference with the demonstrator is that TWIN does not use AGRIF and thus does not have a 1/108° embedded nest. In addition, two other differences must be noted:

- The bathymetries differ over the nested domains[1] (see also Figure 4, sec II.C.1). For TWIN, we use the eNEATL36-only coordinate file (domain_cfg_init.nc, see sec II.C.2) whereas in the demonstrator we use a modified version of this coordinate file for AGRIF.
- The TWIN simulation uses no local drag increase over the parent domain.

- *Satellite and in-situ observations*

The eNEATL36 + AGRIF simulation is validated against in-situ and satellite observations available from the Copernicus Marine Service (CMEMS) catalogue. To make the model data comparable with the observations, we use an external observation operator tool (used internally at MOI). The tool works in an offline way. It reads the observation and errors from the observation files (SLA / SST / SSS and in-situ vertical profiles) and the outputs of the model and create netcdf files containing the model equivalent in the observation space. The observations datasets used for the demonstrator validation are presented in Table 2.

[1] Over the parent domain, the demonstrator bathymetry is computed from the child bathymetry (see sec II.B). The interpolation of the child land sea mask on the parent domain can result in pathologic grids (on the parent domain) that can cause stability issues (when used in non-AGRIF simulations). Note that this is not an issue in AGRIF simulations since the prognostic variables are computed on the child (non-pathologic) grid and then interpolated on the parent domain.

Observation	*Product name*	*Product type (L3/L4)*	*Details and reference*
Sea Surface Temperature (SST)	*ODYSSEA*	*L3S*	*Reference: Piolle et al., (2010)*
Sea Surface Salinity (SSS)	*ESACCI*	*L4*	*Reference: https://climate.esa.int/fr/projects/sea-surface-salinity/ - DOI:10.5285/5920a2c77e3c45339477acd31ce62c3c*
Sea Level Anomaly (SLA)	*AVISO*	*L3 – multiproduct*	*- 3 satellites selected: Jason 3, SARAL / Altika and Sentinel-3A Reference: http://aviso.altimetry.fr"*
Mean Dynamic Topography (MDT)	*CNES-CLS18 MDT*	*L4*	*Reference: Mulet et al., (2021)*
Temperature & Salinity vertical profiles	*CORIOLIS*	*L2*	*Reference : https://doi.org/10.48670/moi-00039*

Table 2 : Observations used to validate the simulation

III. Results

A. First results on the eNEATL36 configuration: comparison between NEMO4.0 and NEMO4.2

Before studying the impact of kilometric resolution, the NEMO version should be validated. Therefore, this section aims to present a comparison between NEMO pre-IMMERSE (4.0) and post-IMMERSE versions (4.2) on the eNEATL36-only configuration. It is divided in two parts. The first part of this section is dedicated to the validation of the NEMO 4.2 version on the eNEATL36 configuration, and the second part presents a comparison of the code performance between NEMO pre (4.0) and post (4.2) IMMERSE versions.

1. NEMO4.2 – Validation

We present here a validation of the NEMO 4.2 version on the eNEATL36 configuration. This is done by comparing two twin simulations (eNEATL36-4.2 and eNEATL36-4.0) over the 2017/01/04 – 2017/12/31 period. The simulations only differ by the version of NEMO used (4.2 or 4.0). They are initialized by the same restart file from the PSY4V3R1 analysis (Lellouche et al., 2018), use the same atmospheric forcing (IFS) and lateral boundary conditions (PSY4V3R1) and use the same parameterizations and physical schemes. Both simulations use the former z* implementation (e.g. "VVL" or "Variable Volume Layer") as vertical coordinate. Since both simulations uses a very similar setup, the simulated physical quantities must be very similar between both simulations.

Figure 7 represents the differences in Sea Surface Temperature (SST, °C) and Kinetic Energy (cm^2/s^2) between eNEATL36-4.2 and eNEATL36-4.0 averaged over the whole period of simulation and the time series of the mean value (averaged over the eNEATL36 domain) of these variables. The differences in SST are small (~ 0.2°C) and occur at mesoscales. The KE is also different at mesoscale for these variables. However, the KE and the SST have the same temporal variability and are very similar at large scale between both simulations. Therefore, updating NEMO version does not have a significant impact on the ocean large scale. Differences seen essentially come from the decorrelation of the two simulations at eddy scales.

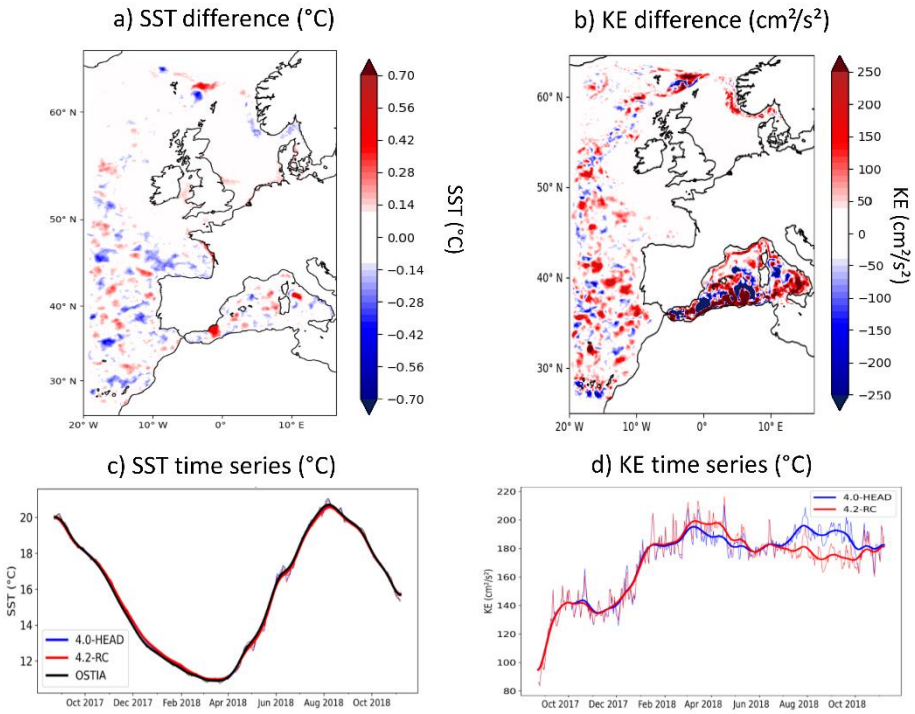

Figure 7 : a) and b), 2D maps of the mean SST (°C) and KE (cm²/s²) difference between eNEATL36-4.2 and eNEATL36-4.0 simulations, averaged over the whole period of simulation. c) and d), time series of the mean SST (°C) and KE (cm²/s²) averaged over the whole IBI area from eNEATL36-4.2 (red) and eNEATL36-4.0 (blue) simulations and from the OSTIA SST dataset (black).

2. *Performance comparison*

A main task of IMMERSE was to improve the overall code performance of NEMO on HPC computers. We investigate here the differences in computational cost between pre (4.0) and post (4.2) IMMERSE NEMO versions on the eNEATL36-only configuration.

We performed two sets of 7-day simulations using the same parameterizations, schemes, and boundary conditions:

- *4.0-HEAD: using NEMO 4.0 version and VVL (Variable Volume Layer) as vertical coordinate*
- *4.2-RC: using NEMO 4.2 and the new vertical coordinate QCO (Quasi-eulerian Coordinate) developed in IMMERSE.*

The sets of simulations were performed using either IFS or ERA-Interim as atmospheric forcing. For each set, we ran simulations while only varying the number of processors used for NEMO, from 1240 to 15000 processors. 5 simulations were launched for each number of processors to have an estimation of the elapsed time variability. For all simulations, the number of processors used along i (*jpni*) and j (*jpnj*) axes is forced so that no suppression of land processors is enabled. As we aim to focus on the on the NEMO code performance, no outputs are written with xios in the simulations. We perform the tests on the Météo-France supercomputer (Belenos).

Figure 8a represents the average simulated year per day (SYPD) against the number of processors used to perform the simulations, and the percentage of improvement of the SYPD in NEMO 4.2 simulations compared to NEMO 4.0 simulations. Simulations using ERA-Interim as atmospheric forcing are a ~2 times faster than simulations using IFS. This is mostly because IFS is read at much higher spatial (~8km for IFS against ~80km for ERA-Interim) and temporal (1h for IFS against 3h for ERAi) resolution.

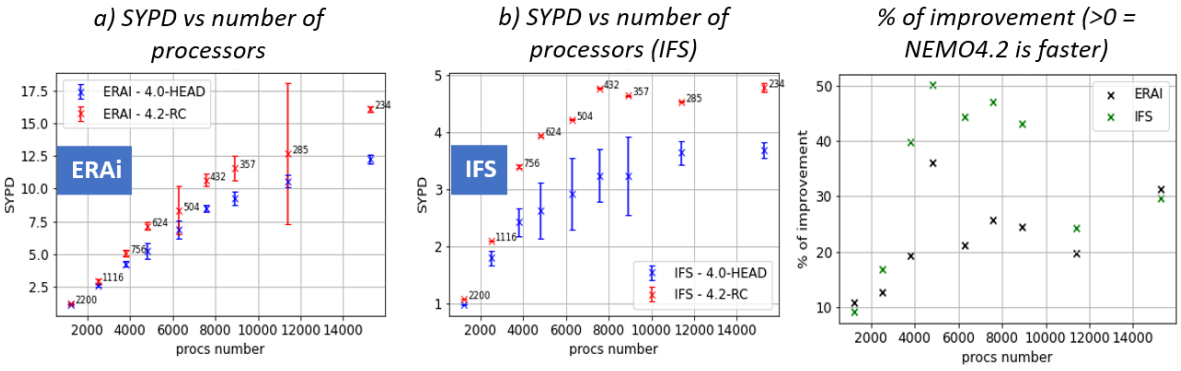

*Figure 8: a) and b) Mean simulated year per day (SYPD) against the number of processor used for a) simulations using ERA-Interim b) IFS as atmospheric forcing, for simulations using NEMO4.0 and VVL as vertical coordinate (blue) and using NEMO4.2 and QCO as vertical coordinate (red), c) the percentage of improvement (100 * [SYPD(NEMO4.2) - SYPD(NEMO4.0)]/ SYPD(NEMO4.0)) for simulations using ERA-interim (black) and IFS (green) as atmospheric forcing.*

The percentage of improvement is above 0 for all number of processors used, meaning that NEMO 4.2 is faster than NEMO 4.0 for all simulations. Stronger improvements (40% to 50%) of the SYPD are found for simulations using a large number of processors (> 3500) and IFS as atmospheric forcing. Simulations are 10% to 50% (resp. are 10% to 35%) faster in NEMO 4.2 when IFS (resp. ERA-Interim) is used as forcing.

We made similar tests using a linear free surface instead of VVL or QCO coordinates for both NEMO4.2 and NEMO4.0 versions (Not shown). We found similar results but with a smaller increase of the SYPD in NEMO 4.2 (5% to 30% when IFS is used as atmospheric forcing). Thus, approximately 30% to 40% of the computational time improvement found in NEMO4.2 can be attributed to the use of QCO instead of VVL as vertical coordinate, whereas the other part is due to a fastening of the NEMO code (code simplification, improvement of the communications, etc …) in its version 4.2.

B. Assessment of the nested configuration

In this section, we provide a validation of the eNEATL36 + Bizoo demonstrator simulation. First, we compare the simulation in terms of computational and storage cost to an eNEATL36 simulation without AGRIF. Then a second part is dedicated to the assessment of the two-way nesting over the demonstrator simulation. Finally, the demonstrator simulation is validated from a macroscopic point of view.

1. Performance comparison

Table 3 represents the elapsed time for a 7-day simulation on the meteo-france supercomputer Belenos on the eNEATL36 only and eNEATL36 + Bizoo configuration. Overall, the initialisation time is two times longer for the eNEATL36 + Bizoo configuration. The computing time is 9 to 10 times longer for the nested configuration than for the configuration without nest, which is roughly consistent to the ratio between the number of operations performed in eNEATL36 + BIzoo and eNEATL36, which is 9.4 ($\frac{N_{points}(eNEATL36)+N_{points}(BIzoo)*3}{N_{points}(eNEATL36)} = 9.4$).

Configuration	*Elapsed time on 3740 processors – no XIOS outputs*		*Elapsed time on 3740 processors – with XIOS outputs*	
	Initialisation time	*Computing time*	*Initialisation time*	*Computing time*
eNEATL36	*~3 min*	*~7 min*	*~3 min*	*~7 min*
eNEATL36 + Bizoo	*~4 min*	*~66 min*	*~4 min*	*~70 min*

Table 3 : Elapsed time on the meteo-france supercomputer (Belenos) for a 7-day simulation on 3740 processors for NEMO and 100 processors for XIOS.

2. Two-way nesting assessment

Interactions between the parent and the child grid are two-way, in the sense that both the parent and the child model solution interact with each other. Nevertheless, we must ensure that oceanic structures are transmitted with as few artefacts as possible when advected through the nest boundaries, and that the boundaries do not block nor reflect the internal waves passing through the boundaries.

- *Balanced motions*

Figure 9 shows the evolution of the vorticity structures near the western Bizoo boundary at the early stages of the simulation. Although there are much more small-scale vorticity structures inside the nest area than outside, the vorticity structures are well preserved when they pass across the nest boundaries. It shows that the two-way nesting allows, at least qualitatively, balanced motions to be transmitted through the nest boundaries.

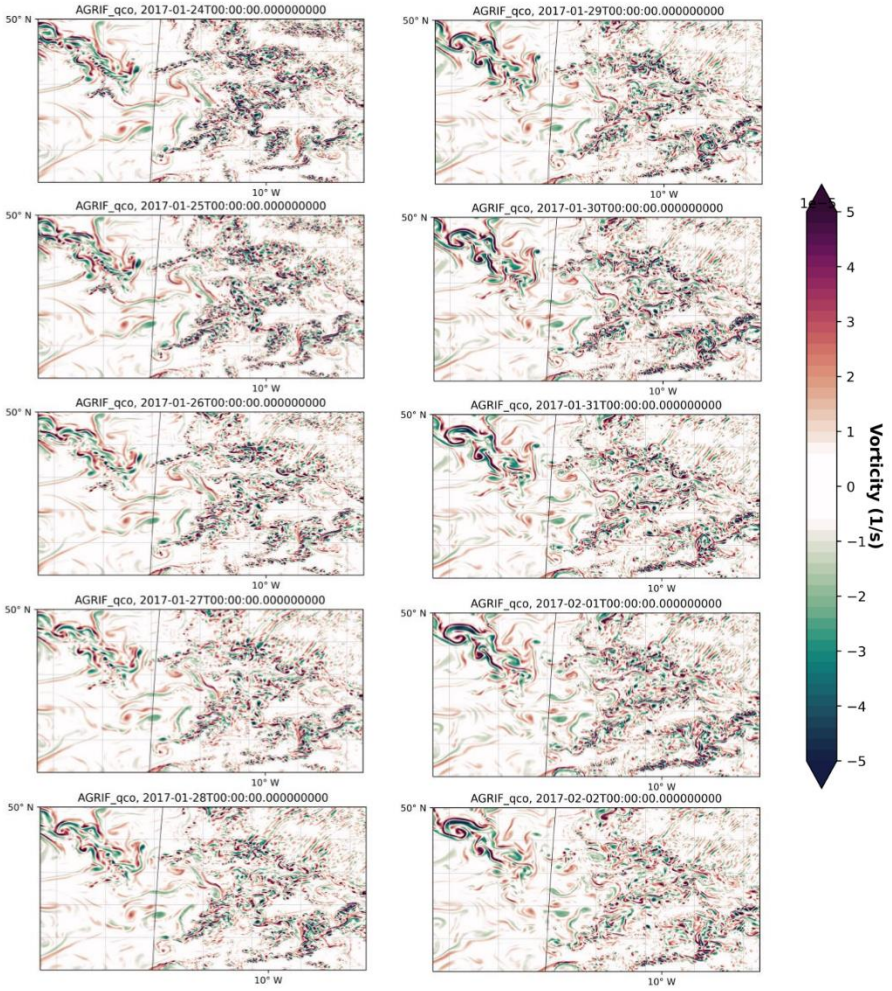

Figure 9: Snapshots of daily averages of the current vorticity (in s^{-1}) near the western AGRIF108 boundaries for january 24th to ferburay th 2th. The black line represents the nest boundary

- *Internal waves*

The Iberian continental slope is an intense spot of tidal internal waves generation. These generally propagate offshore with average phase speeds for the 1st mode around 3 m/s. This is exemplified in Figure 10 which represents the hoevmoller plot (time vs longitude) of the vertical velocities at 200m depth on this section. On this section, internal waves are generated along the slope of the continental shelf at 5.5°W approximately and propagate westward until they cross the nest boundary at 13.5°W approximately.

Transmitting (and eventually absorbing unresolved) internal wave motions is not particularly covered in the two-way nesting literature. Methodologies in the case of one-way nesting have been recently proposed by Rogers et al. (2019). Here a qualitative inspection of vertical velocities associated to these internal waves show that they are strongly reduced when they cross the boundary, but reflections are hardly noticed. This change in vertical velocity is mostly due to the change in resolution (and to the sponge layer bordering the child domain): internal waves outside the nest are not resolved as well as inside the nest. However, the waves are not reflected by the boundaries and are able to propagate across.

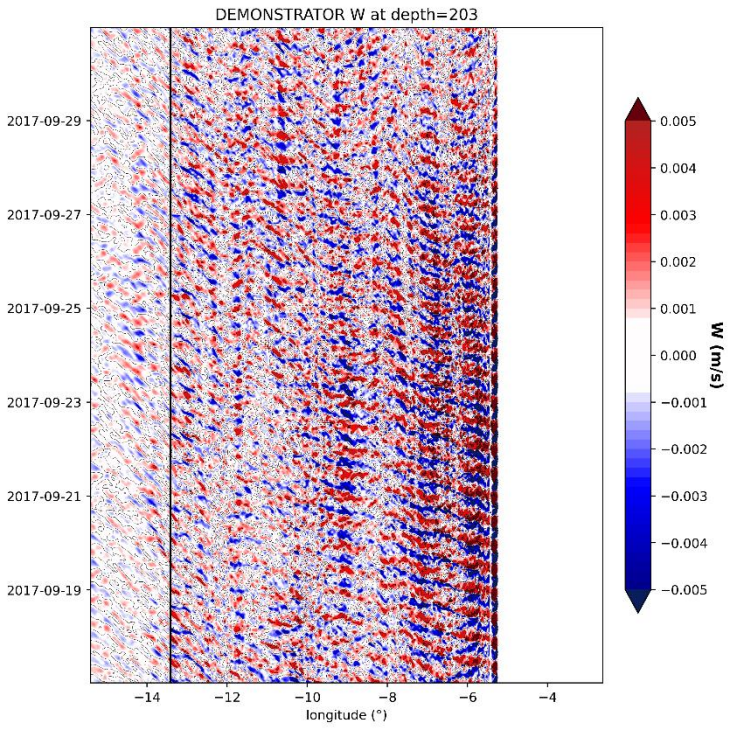

Figure 10 : Hoevmoeller diagram (time vs longitude) of the vertical velocities (m/s) at 200m and 46.5°N. The dark line represents the western nest boundary.

3. *Macroscopic validation*

As in previous section the good behaviour of the nest has been shown regarding the two-way nesting, we can provide in this section a validation of the eNEATL36 + Bizoo demonstrator simulation from a macroscopic point of view. The simulation is validated against satellite and in-situ observation and is compared to a twin simulation with no nest (TWIN). As our simulation is a free run, in the sense that we don't use any data assimilation, the validation is only statistical.

- *Tidal solution*

The demonstrator tidal solution is validated against the FES 2014 (Lyard et al., 2021) and is compared to the TWIN solution.

Figure 11 represents the amplitude and phase of the M2 and S2 tidal harmonics for the two simulations and FES 2014. The tidal solution in the demonstrator simulation is continuous inside and outside the zoom. This shows that the tidal waves are efficiently transmitted when they cross the nest boundaries.

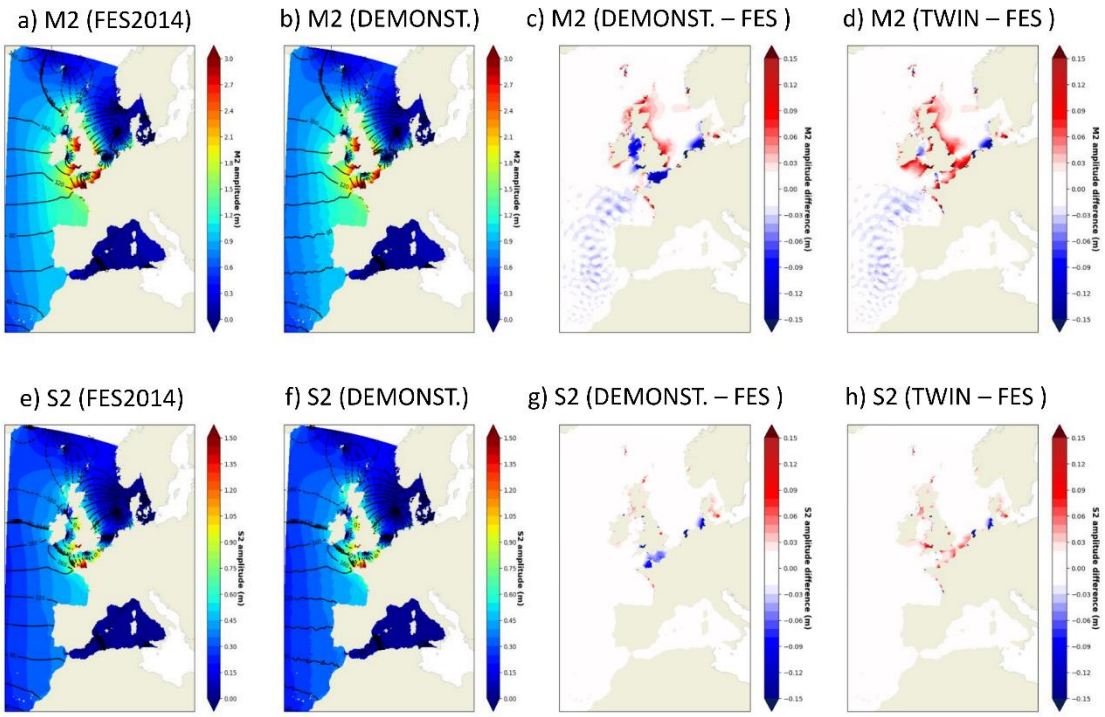

Figure 11 : a), b), M2 and e), f) S2 tidal amplitude (colours) and phase (contours) for FES2014 (a, e) and the demonstrator simulation (b and f) and differences between DEMONSTRATOR and FES for M2 and S2 amplitude (c and g respectively) and between TWIN and FES (d and h respectively)

A good agreement is found for both M2 and S2 components between the phase simulated by eNEATL36 + Bizoo demonstrator simulation and FES2014 data. The amplitude difference between the nested simulation and FES2014 is small and inferior to ± 15cm everywhere for both S2 and M2. The strongest differences are found in the Channel and near English coasts. Over the Channel, the M2 amplitude is underestimated by ~10 cm in eNEATL36 + Bizoo, whereas it is overestimated by the same amount in the TWIN simulation. This discrepancy between the tidal solution is not necessarily related to the nest but is more likely related to the use of a drag coefficient boost in the demonstrator simulation and to the change of bathymetry between both simulations (see sec II.C.1). The RMSEs with FES2014 on the amplitude of M2, S2, K1, O1 and M4 tidal harmonics are close in DEMONSTRATOR and TWIN simulations (Table 4). We can conclude that the nested configuration simulates a tidal solution as realistic as a twin simulation with no nest.

Simulation		*M2*	*S2*	*K1*	*O1*	*M4*
DEMONSTRATOR	*Mean Bias (cm)*	*-1.48*	*-0.48*	*-0.23*	*-0.05*	*-0.31*
	Mean RMSE (cm)	*1.81*	*0.65*	*0.28*	*0.13*	*0.38*
TWIN	*Mean Bias (cm)*	*-0.69*	*-0.13*	*-0.19*	*-0.05*	*-0.01*
	Mean RMSE (cm)	*1.75*	*0.63*	*0.26*	*0.14*	*0.30*

Table 4 : Mean bias and RMSE with FES2014 for M2, S2, K1, O1 and M4 tidal harmonics over the nest area for DEMONSTRATOR and TWIN simulations.

- *Temperature and Salinity*

We validate the Sea Surface Temperature (SST) and Salinity (SSS) against the ODYSSEA SST (Piolle et al., 2010) and ESACCI SSS (Boutin et al., 2020) datasets respectively. Figure 12 represents the mean SST(°C) differences and RMSE of the eNEATL36 + Bizoo demonstrator simulation with the observations, the mean difference with TWIN and the associated time series.

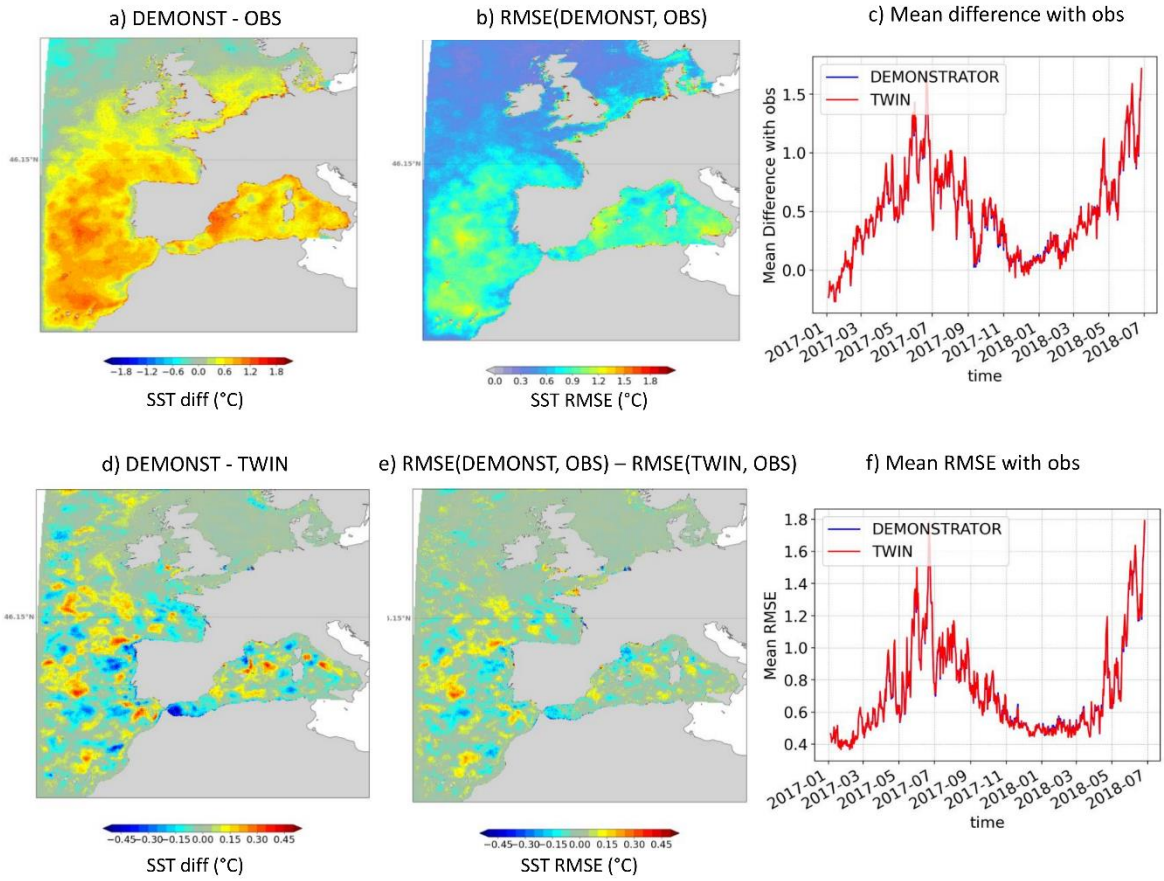

Figure 12 : Maps of the mean difference (a) and RMSE (b) in SST (°C) with observations for DEMONSTRATOR, averaged over the whole period of simulation. Maps of the mean difference between DEMONSTRATOR and TWIN (d) and between the RMSEs of DEMONSTRATOR and TWIN (e). (c) and (f) represents the time series of the mean difference and of the mean RMSE with the observations in SST (°C) respectively

First, it is important to mention that the SST solution is continuous across the nest boundaries. This shows that the two-way nesting between the parent and the child grids is effective and allows the SST information to be transmitted across the nest boundaries. When compared with ODYSSEA, the SST simulated by the demonstrator is warmer than the observations in average over the period of the simulation. This warm bias is stronger in summer and reach ~+1.5°C and a RMSE of 1.5°C in July in average over the nest area (Figure 12, c, f). From a spatial point of view, we found the strongest differences in SST between the model and the observations in the Mediterranean Sea and on the open waters south west of the Portuguese coast. The demonstrator SST is however relatively consistent with observations over the continental shelf and over the Portugal upwelling (Figure 12, a). Most of those differences are not directly related to the nest since they occur in TWIN as well. Indeed, there is no change in SST at large scales between TWIN and DEMONSTRATOR. The differences between the two

simulations are related to changes in the mesoscale activity and are relatively small (< ± 0.5°C) (Figure 12, d). We can note a slight improvement of the RMSE on SST over the continental shelf and over the Alboran gyre in DEMONSTRATOR in comparison of TWIN (Figure 12, e).

Regarding the SSS, the ESA-CCI product contains strong uncertainties near coasts (Boutin et al., 2020). Thus, we use this product to validate the SSS only on regions that are sufficiently away from coasts (~200km from coasts). Over the Atlantic, the model SSS is close to the observations, with a mean RMSE < 0.1 psu (Figure 13). The SSS from the demonstrator simulation is consistent with TWIN. We can note some differences in SSS between the two simulations off the coasts of Portugal, with slightly more freshwater in the demonstrator simulation than in TWIN. Such a difference may be related to a change in upwelling-related mesoscale activity and will be investigated in the IMMERSE deliverable D6.3. In conclusion, the SSS simulated by the demonstrator simulation is consistent with observations, and the differences in SSS between the demonstrator and the twin simulation show that the nest does not have a strong impact on the large scale SSS.

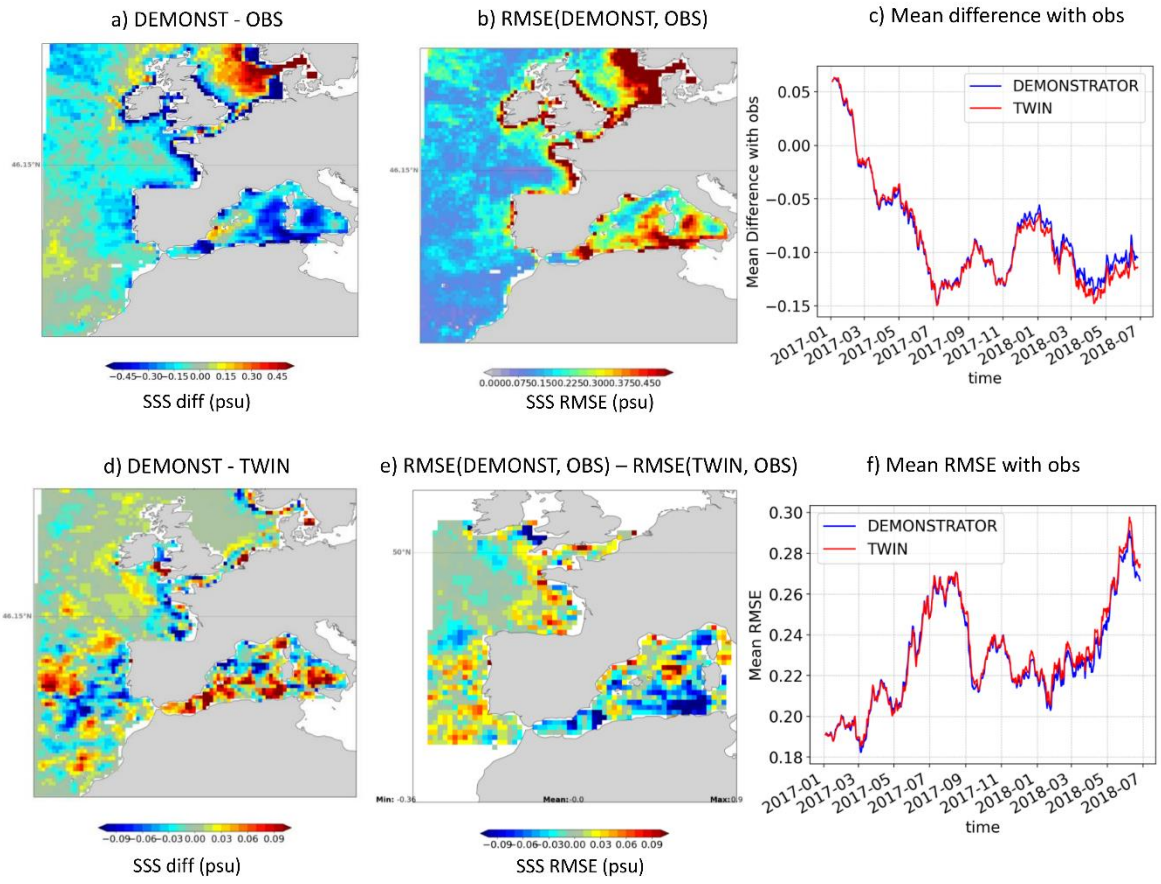

Figure 13: Same as Figure 10, but for the Sea Surface Salinity (in psu).

Model temperature and salinity are collocated on CORIOLIS T & S in-situ profiles using an external observation operator (see sec. III.B.1).Figure 14 represents mean bias and RMSE with the observations for the salinity and the temperature at every model level, averaged over the nest area. On average, the model is warmer than the observations over the first 500m, and colder at depth. The highest differences in temperature are found in the first 500m. This is not surprising, given that the upper ocean layers are the most impacted by surface processes, and thus have the highest temporal variability.

For the salinity, we observe a fresh bias within the first 1000m in both demonstrator and TWIN simulations. This bias is not related to the nest, as the mean bias and RMSE with observations simulation are very close between the demonstrator simulation and TWIN. Thus, the high-resolution nest has a very small impact on the mean state of salinity. In conclusion, the nested model solution is continuous across the nest boundaries and as realistic as a simulation with no nest in terms of temperature and salinity.

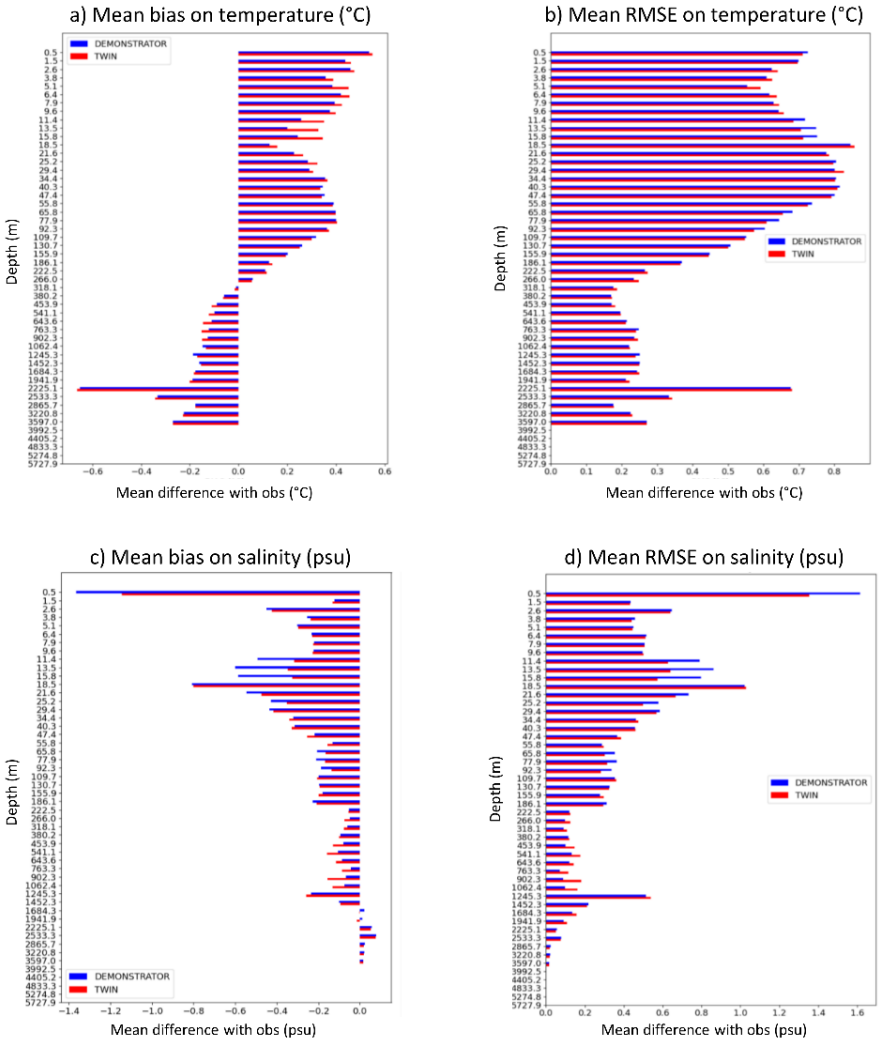

Figure 14: a) Mean temperature (°C) and c) salinity (psu) difference and b) Mean temperature (°C) and d) salinity (psu) RMSE with the CORIOLIS T & S profiles at every model level, averaged over the nest area.

- *Sea Surface Height (SSH) / Sea level anomaly (SLA)*

We validate the Sea Surface Height (SSH) against AVISO Sea Level Anomaly (SLA) data. Since the demonstrator simulation represents tidal motions, we kept the AVISO SLA unfiltered from tides. We selected 3 satellites for which the data were available over the whole period of simulation: Jason 3, SARAL / Altika and Sentinel-3A. The observation operator tool described in sec III.B.1 is used to interpolate the model data on satellite tracks. Note that the tool performs (when necessary) linear temporal and bilinear spatial interpolations to replace the model data on the observation space and that those interpolations can induce errors in regions of high tidal range.

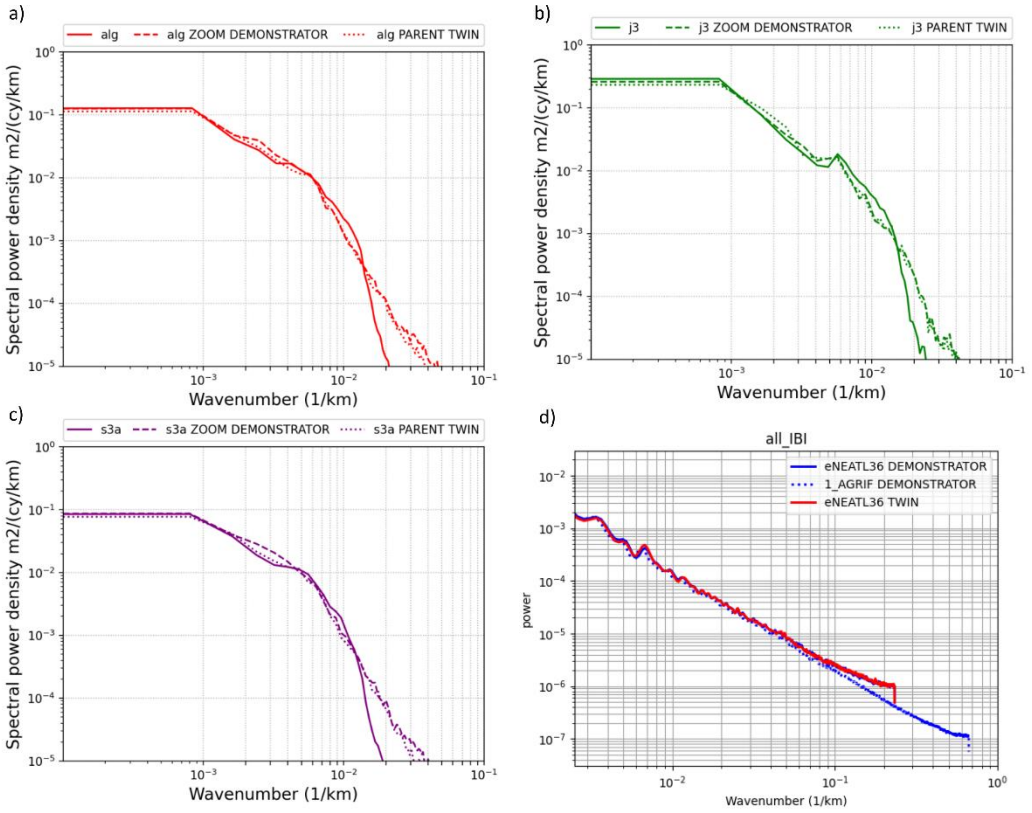

Figure 15 : Along-track sea level anomaly spectrums, computed for a) SARAL / Altika b) Jason 3 and c) Sentinel-3A satellites and d) total SSH spectrum computed directly from 2D model data (with on-track interpolation) for TWIN (red), DEMONSTRATOR parent (blue, solid line) and child (blue, dotted) grid. The solid line represents the spectrum computed from observed along track satellite SLA and the dashed and dotted lines represent respectively the spectrum computed from DEMONSTRATOR and TWIN simulations data, which have been colocalized with the satellite observations beforehand.

Figure 15 represents the observed and simulated SLA spectrums for all three satellites, computed directly over satellite tracks. The demonstrator simulation SLA spectrum is very consistent with the observed spectrum for scales above ~100km, which shows that such scales are resolved realistically by the simulations. Below 100km, the observed SLA spectral power density drops rapidly since the considered scales are below the effective resolution of the satellites (Ballarotta et al., 2019). Consequently, such data cannot be used to validate the SLA spectrums at scales below 100km. Note that future satellite missions such as SWOT (Fjørtoft et al., 2014) will have a higher effective resolution that will facilitate the validation of the SLA at smaller scales.

The model SLA is interpolated on the satellite tracks that have a resolution of ~7km, which deteriorates the effective resolution of the data. In addition, a filter is applied on the small scales by the observation operator. Thus, SLA spectrums of DEMONSTRATOR and TWIN are very close at high resolutions (< 100km) since the smaller scales resolved only by the nested simulation are filtered by the colocalization operations made on the data. The full SSH spectrum computed directly from the model outputs (Figure 15, d) confirms this as it shows that the differences in spectrum between TWIN and DEMONSTRATOR occur at scales < 10km. On larger scales, the SLA spectrums of TWIN and DEMONSTRATOR are very close. Thus, the high-resolution nest does not have a strong impact on SLA at such scales.

- *Transports across the Gibraltar strait*

The Gibraltar strait connects the Atlantic Ocean to the Mediterranean Sea and has a large influence on the oceanic circulation in the area. Therefore, it is of concern to validate the transports across the strait simulated by the nested configuration, in comparison with TWIN and the values given by the literature. Figure 16 represent the South-North section across the eastern part of the Gibraltar strait of the along-strait current velocity at ~5.4°W from Baschek et al. (2001) and from the two simulations (DEMONSTRATOR and TWIN). Note that the orientation of the cross-section is slightly different between the simulations and Baschek et al. (2001), as we extracted the cross-section in the simulation by selecting points along the y axis by fixing the x axis point for a matter of simplicity.

Thanks to the higher resolution in the demonstrator simulation, the strait is much better defined than in TWIN. Over the section in Figure 16, the along-strait current maximum for the Mediterranean outflow (negative values) is located between 200 and 450m in the TWIN simulation (Figure 16, d). In the demonstrator simulation the Mediterranean outflow vein goes much deeper, and the along-strait current maximum goes down to 700m (Figure 16, b). This is more consistent to the inverse tidal model solution from Baschek et al. (2001) (Figure 16, c) where the mean Mediterranean outflow is separated in two veins, a first one at ~300m depth and a deeper one at ~650m. The Atlantic water inflow (positive values) is simulated realistically by both TWIN and DEMONSTRATOR simulations in comparison with Baschek et al. (2001) ADCP measurements and inverse tidal model (Figure 16).

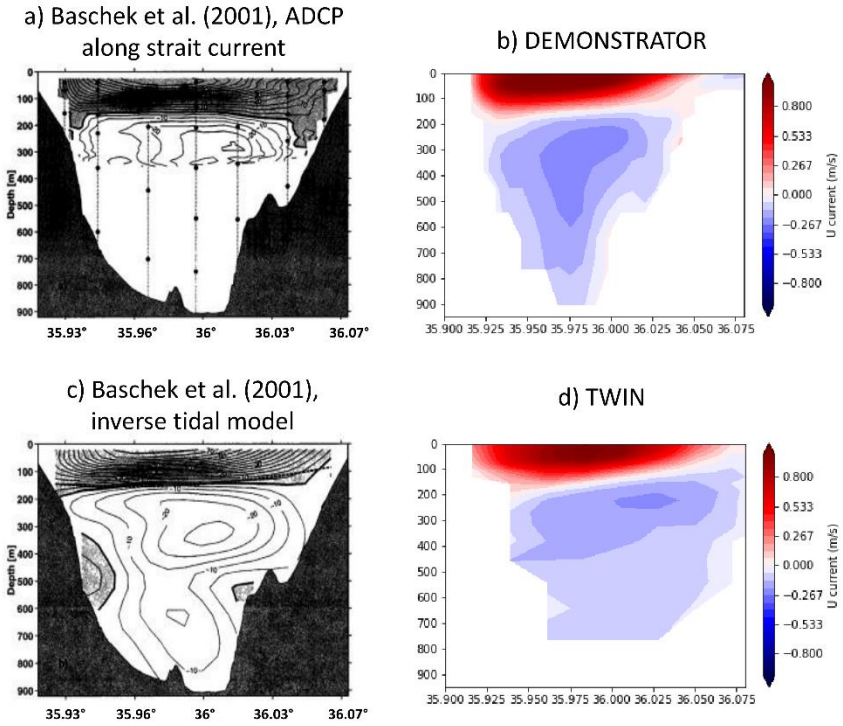

Figure 16: Mean along strait current in cm/s along a north-south section across the Gibraltar strait at ~5.4°W from a) and c) Baschek et al., (2001) obtained from ADCP measurement and an inverse tidal model respectively and c) and d) for the DEMONSTRATOR and TWIN simulations respectively.

We compute the transports across the Gibraltar strait through a South-North cross-section located at Tarifa. The mean Mediterranean inflow in TWIN and DEMONSTRATOR is consistent with the highest estimations from the literature (see Criado-Aldeanueva et al., 2012 for a review). Thus, it may be slightly overestimated as most studies give an estimation of the Mediterranean inflow between 0.8 and 0.9 Sv. The inflow is slightly reduced in the demonstrator simulation compared to TWIN, so it is more consistent with the literature estimates. The Mediterranean Outflow is also slightly overestimated when compared to observations (Marullo et al., 2016; Bryden et al., 1994; García-Lafuente et al., 2011; Baschek et al., 2001). This overestimation is nonetheless slightly reduced in DEMONSTRATOR compared to TWIN. Finally, the net flow is positive in the simulations as in the literature estimates (see Criado-Aldeanueva et al., 2012 for a review) but is also overestimated for both simulations. However, the net flow is highly dependent on the SSH prescribed on the eNEATL36 open boundary conditions (Soto-Navarro et al., 2015). A better agreement with literature estimates of the net flow can be achieved by correcting the SSH on the eNEATL36 open boundary conditions.

	Inflow (Sv)	*Outflow (Sv)*	*Net flow (Sv)*	*Section area (m^2)*
DEMONSTRATOR	*1.08*	*-0.83*	*0.24*	*6.312*
TWIN	*1.12*	*-0.91*	*0.2*	*6.530*
Litterature estimates	*1.2-0.7*	*-0.6 - -0.9*	*0.03 – 0.08*	

Table 5 : Mean Mediterranean inflow, ouflow and net flow across the Gibraltar strait computed from a South-North section at Tarifa.

IV. Conclusion and perspectives

This deliverable (6.1) is dedicated to the description of the eNEATL36 + BIzoo high – resolution configuration (https://github.com/immerse-project/eNEATL36-BIzoo_Demonstator) and to the validation of a demonstrator simulation on this configuration from a macroscopic point of view.

In a preliminary work, we compared NEMO 4.0 and NEMO 4.2 versions on two twin eNEATL36 configurations. We showed that updating the NEMO version does not have an impact on the ocean mean state. We also performed scalability tests to compare the computational cost of the two NEMO versions. Our results show that NEMO 4.2 is 10 to 50% faster than NEMO 4.0. About 20 to 30% of this improvement comes from the change of the vertical coordinate in NEMO 4.2 (QCO instead of VVL).

The kilometric-resolution nested configuration eNEATL36 + BIzoo was then successfully implemented in NEMO 4.2 version. A 1.5-year demonstrator simulation from January 2017 to July 2018 has been performed and validated against satellite and in-situ observations and a twin simulation with no nest.

Qualitative assessment shows that both balanced and wave motions are smoothly transmitted through the two-way nested grids. Quantitatively, energetic diagnostics, global drifts and comparison to observations do not reveal any artefact due to the nesting procedure, which validates the AGRIF methodology in NEMO 4.2.

The demonstrator simulation tidal, SLA and SSS solution is realistic at large scales when compared to the observations. The tidal amplitude is slightly underestimated in our demonstrator simulation, but this underestimation is more likely to originate from the combined effect of the drag increase used in the demonstrator simulation and to the bathymetry than from the nesting procedure itself. For the SST, we observe a warm bias with the observations in both the demonstrator and the twin simulations. It is likely to originate whether from the forcing, the bulk, the penetrative solar radiation parameterisation, or the vertical mixing parameterisations used in both setups. Thanks to the increased resolution, the demonstrator simulation, the Mediterranean inflow and outflow are more consistent with the literature estimates than in the eNEATL36-only configuration.

The demonstrator simulation data will be shared to IMMERSE project collaborators and will be available on demand for collaborators outside the IMMERSE project. Thereafter, the work on the eNEATL36 + BIzoo will proceed within the context of the IMMERSE deliverable 6.3 and will focus on the small scales simulated by the nested configuration. In particular, the surface oceanic currents will be validated against in-situ and high-frequency radar observations. The impact of the high-resolution nest on the ocean dynamics will also be assessed by continuing the comparison between the demonstrator and the twin eNEATL36-only simulation.

References

Adcroft, A. and Campin, J.-M.: Rescaled height coordinates for accurate representation of free-surface flows in ocean circulation models, Ocean Modelling, 7, 269–284, https://doi.org/10.1016/j.ocemod.2003.09.003, 2004.

EMODnet Digital Bathymetry (DTM 2018): https://sextant.ifremer.fr/geonetwork/srv/api/records/18ff0d48-b203-4a65-94a9-5fd8b0ec35f6, last access: 8 April 2022.

Ballarotta, M., Ubelmann, C., Pujol, M.-I., Taburet, G., Fournier, F., Legeais, J.-F., Faugère, Y., Delepoulle, A., Chelton, D., Dibarboure, G., and Picot, N.: On the resolutions of ocean altimetry maps, 15, 1091–1109, https://doi.org/10.5194/os-15-1091-2019, 2019.

Baschek, B., Send, U., Lafuente, J. G., and Candela, J.: Transport estimates in the Strait of Gibraltar with a tidal inverse model, 106, 31033–31044, https://doi.org/10.1029/2000JC000458, 2001.

Boutin, J., Vergely, J., Reul, N., Catany, R., and Josey, S.: ESA Sea Surface Salinity Climate Change Initiative (Sea_Surface_Salinity_cci): weekly and monthly sea surface salinity products, v2.31, for 2010 to 2019, https://doi.org/10.5285/4ce685bff631459fb2a30faa699f3fc5, 2020.

Brodeau, L., Barnier, B., Gulev, S. K., and Woods, C.: Climatologically Significant Effects of Some Approximations in the Bulk Parameterizations of Turbulent Air–Sea Fluxes, 47, 5–28, https://doi.org/10.1175/JPO-D-16-0169.1, 2017.

Bryden, H. L., Candela, J., and Kinder, T. H.: Exchange through the Strait of Gibraltar, Progress in Oceanography, 33, 201–248, https://doi.org/10.1016/0079-6611(94)90028-0, 1994.

Criado-Aldeanueva, F., Soto-Navarro, F. J., and García-Lafuente, J.: Seasonal and interannual variability of surface heat and freshwater fluxes in the Mediterranean Sea: budgets and exchange through the Strait of Gibraltar, 32, 286–302, https://doi.org/10.1002/joc.2268, 2012.

Debreu, L. and Blayo, E.: Two-way embedding algorithms: a review, Ocean Dynamics, 58, 415–428, https://doi.org/10.1007/s10236-008-0150-9, 2008.

Fjørtoft, R., Gaudin, J.-M., Pourthié, N., Lalaurie, J.-C., Mallet, A., Nouvel, J.-F., Martinot-Lagarde, J., Oriot, H., Borderies, P., Ruiz, C., and Daniel, S.: KaRIn on SWOT: Characteristics of Near-Nadir Ka-Band Interferometric SAR Imagery, 52, 2172–2185, https://doi.org/10.1109/TGRS.2013.2258402, 2014.

García-Lafuente, J., Sánchez-Román, A., Naranjo, C., and Sánchez-Garrido, J. C.: The very first transformation of the Mediterranean outflow in the Strait of Gibraltar, 116, https://doi.org/10.1029/2011JC006967, 2011.

Lellouche, J.-M., Greiner, E., Le Galloudec, O., Garric, G., Regnier, C., Drevillon, M., Benkiran, M., Testut, C.-E., Bourdalle-Badie, R., Gasparin, F., Hernandez, O., Levier, B., Drillet, Y., Remy, E., and Le Traon, P.-Y.: Recent updates to the Copernicus Marine Service global ocean monitoring and forecasting real-time 1⁄12° high-resolution system, 14, 1093–1126, https://doi.org/10.5194/os-14-1093-2018, 2018.

Lyard, F. H., Allain, D. J., Cancet, M., Carrère, L., and Picot, N.: FES2014 global ocean tide atlas: design and performance, 17, 615–649, https://doi.org/10.5194/os-17-615-2021, 2021.

Madec, G., Bourdallé-Badie, R., Chanut, J., Clementi, E., Coward, A., Ethé, C., Iovino, D., Lea, D., Lévy, C., Lovato, T., Martin, N., Masson, S., Mocavero, S., Rousset, C., Storkey, D., Müeller, S., Nurser, G., Bell, M., Samson, G., Mathiot, P., Mele, F., and Moulin, A.: NEMO ocean engine, https://doi.org/10.5281/zenodo.6334656, 2022.

Maraldi, C., Chanut, J., Levier, B., Ayoub, N., De Mey, P., Reffray, G., Lyard, F., Cailleau, S., Drévillon, M., Fanjul, E. A., Sotillo, M. G., Marsaleix, P., and the Mercator Research and Development Team: NEMO on the shelf: assessment of the Iberia–Biscay–Ireland configuration, 9, 745–771, https://doi.org/10.5194/os-9-745-2013, 2013.

Marullo, S., Minnett, P. J., Santoleri, R., and Tonani, M.: The diurnal cycle of sea-surface temperature and estimation of the heat budget of the Mediterranean Sea, 121, 8351–8367, https://doi.org/10.1002/2016JC012192, 2016.

Mulet, S., Rio, M.-H., Etienne, H., Artana, C., Cancet, M., Dibarboure, G., Feng, H., Husson, R., Picot, N., Provost, C., and Strub, P. T.: The new CNES-CLS18 global mean dynamic topography, 17, 789–808, https://doi.org/10.5194/os-17-789-2021, 2021.

Piolle, J.-F., Autret, E., Arino, O., Robinson, I. S., and Le Borgne, P.: Medspiration: Toward the Sustained Delivery of Satellite SST Products and Services over Regional Seas, 686, 361, 2010.

Renault, L., McWilliams, J. C., and Masson, S.: Satellite Observations of Imprint of Oceanic Current on Wind Stress by Air-Sea Coupling, Sci Rep, 7, 17747, https://doi.org/10.1038/s41598-017-17939-1, 2017.

Soto-Navarro, J., Somot, S., Sevault, F., Beuvier, J., Criado-Aldeanueva, F., García-Lafuente, J., and Béranger, K.: Evaluation of regional ocean circulation models for the Mediterranean Sea at the Strait of Gibraltar: volume transport and thermohaline properties of the outflow, Clim Dyn, 44, 1277–1292, https://doi.org/10.1007/s00382-014-2179-4, 2015.